Playing it safe at early life stages: Balancing energy allocations to maximize fitness under seasonal pathogen dynamics

Authors:

Zuania Colón-Piñeiro*, Department of Biology, University of Florida,
colonpineiro.z@ufl.edu, orcid.org/0000-0003-0508-2538;

Nich W. Martin, Department of Entomology and Nematology, University of Florida,
n.martin@ufl.edu, orcid.org/0000-0001-9539-250X;

Travis J Klee, Department of Biology, University of Florida,
tklee@ufl.edu, https://orcid.org/0009-0000-9545-7801;

Brittaney L Buchanan, Department of Biology, University of Florida,
bbuchanan1@ufl.edu;

Colette M St. Mary, Department of Biology, University of Florida, National Science Foundation,
cstmary@nsf.gov, orcid.org/0000-0002-3175-5284;

Miguel Acevedo, Department of Wildlife Ecology and Conservation, University of Florida,
maacevedo@ufl.edu, orcid.org/0000-0002-8289-1497;

Patricia Burrowes, Department of Biology, University of Puerto Rico, National Museum of Natural History, Madrid, Spain, pburrowesupr@gmail.com, orcid.org/0000-0002-3085-6681;

Ana V. Longo*, Department of Biology, University of Florida,
ana.longo@ufl.edu, orcid.org/0000-0002-5112-1246

Running title: Modeling costs of seasonal infections

Keywords: direct-developing amphibians; dynamic state variable model; energetic constraints; host-pathogen interactions; tradeoffs; seasonality in the tropics.

Type of article: Letters

Number of words in the abstract: 149

Number of words in main text (excluding abstract, acknowledgments, references, tables and figure legends): 4,205

Number of references: 84

Number of figures: 4 (+ 4 supplementary)

Number of tables: 1

Number of boxes: 1

Correspondence author: **Zuania Colón-Piñeiro**, email zcolonp@gmail.com, phone (939)633-4705, address 421 Carr Hall 876 Newell Dr. University of Florida Gainesville, FL 3261; **Ana V Longo**, email: ana.longo@ufl.edu, phone (352)214-0882, address 421 Carr Hall 876 Newell Dr. University of Florida Gainesville, FL 3261.

Statement of authorship: conceptualization: ZCP, AVL; model development: ZCP, NWM, CStM, TJK, and BLB; coding and data visualization: NWM, ZCP; data analysis: ZCP, CStM, AVL, PAB, and MAA; funding acquisition: AVL, PAB; writing first draft of the manuscript: ZCP, AVL. All co-authors contributed substantially to revisions and editing the manuscript and approved the final version.

Data accessibility statement: Script developed to generate backward and forward iterations, as well as figures, is available during review via GitHub (https://github.com/ZuaniaColon/Modeling-costs-of-seasonal-infections.git). We will archive it in a public repository such as Dryad once the manuscript is accepted.

Abstract

Infections carry inherent tradeoffs in growing hosts due to the changing demands for resource allocation among key processes (i.e., growth and immunity). We implemented dynamic state variable models to determine which changes in energy allocation maximize fitness in amphibians with enzootic infections. By accounting for seasonality in our mechanistic models, we identified critical windows that maximize individual growth while limiting mortality under increased pathogen burden. The model predicted that seasonality in pathogen exposure and foraging success exacerbate growth-defense tradeoffs, resulting in delayed maturity and lower survival when frogs hatched under sub-optimal environmental conditions. Our simulations support well-known field patterns showing that increased frog reproduction coincides with high resource availability and low pathogen risk. Our models can be further parameterized to understand the effect of emerging diseases under predicted climate change across taxa, and to evaluate the best timing for species re-introductions that would reduce fitness tradeoffs in the population.

Introduction

Immune responses are one of the most critical factors controlling diseases and maintaining homeostasis. Hosts spending resources on immune responses incur in fitness costs associated with decreasing investments in development (Keehnen *et al.* 2021), growth (Korfel *et al.* 2015; Soler *et al.* 2003), and/or reproduction (Brannelly *et al.* 2021a), likely mediating the arms race with pathogen virulence. Tradeoffs between energy-demanding processes have been widely studied across taxa (Brannelly *et al.* 2021b; Grogan *et al.* 2020; Huot *et al.* 2014; Keehnen *et al.* 2021; Korfel *et al.* 2015; Soler *et al.* 2003), and the magnitude of the interactions among the aforementioned processes varies at different scales. Although empirical studies have provided evidence for the effect of energy allocation tradeoffs on individuals' fitness, it is rarely included in disease ecology models.

To understand tradeoffs in disease ecology, susceptible and infected models have been broadly applied to predict pathogen spread using individual's abundance (Alizon *et al.* 2009; DiRenzo *et al.* 2019; Drewry 1970; Dushoff 1999; Miller *et al.* 2005; Simon *et al.* 2022; Stephenson *et al.* 2017). These models assume that individuals come from homogeneous populations, ignoring sources of variability. For example, incorporating host demography shows that the stabilization of a population after an outbreak depends on the age structure (Simon *et al.* 2022). In fact, we can develop mathematical models to directly test the strategies that increase host fitness when pathogens are already established in the population. Because the outcome of an outbreak is context-dependent, an agent-based approach is necessary to better understand the factors driving population dynamics.

Dynamic optimization models can identify the optimal defense strategy (i.e., a strategy that minimizes the cost of infection) at the individual level (Shudo & Iwasa 2004). These models are built considering the underlying process of the observed relationships; thus, we can use them to express a hypothesis mathematically and hence provide predictions for comparison

to empirical patterns (Mangel & Clark 1988; McCauley *et al.* 2000). Here, we used dynamic optimization models to evaluate how the growth-defense energy allocation tradeoff affected individuals' fitness.

Although pathogens and parasites evidently trigger tradeoffs between energy-demanding processes, the magnitude of their effect on fitness varies among life history stages and environmental conditions. Life history theory predicts pre-reproductive allocation strategies will determine future fitness by influencing the state (phenotype) of an individual at maturity (McNamara & Houston 1986; Stearns 2000). At early life stages, pathogen exposure can have carryover effects on survival by affecting condition-dependent traits like growth, even after individuals successfully clear infections (Burrowes *et al.* 2008; Garner *et al.* 2009; Rumschlag & Boone 2020). On the other hand, pathogen exposure and infection are often mediated by environmental conditions such as seasonality. Indeed, seasonal disease outbreaks are pervasive across animal and plant communities (Altizer *et al.* 2006). Changes in abiotic conditions modulate critical aspects of activating immune responses against pathogens (Le Sage *et al.* 2021) and the recruitment of beneficial symbionts from the environment (Altizer *et al.* 2006; Longo *et al.* 2015; Nelson 2004). Seasonality also mediates vector abundance and behavior (Agha *et al.* 2017; Nguyen *et al.* 2019), which in turn affects host-pathogen or parasite interactions. In addition, shifts in resource availability (Rumschlag & Boone 2020; Stewart & Woolbright 1996) and host foraging success (Alvarado-Rybak & Azat 2021; Rumschlag & Boone 2020) between seasons may result in variation in nutritional status with further effects on growth, development (Guyer 1988; Schiesari *et al.* 2006), and the maintenance of the immune system (Huang *et al.* 2020; Merino *et al.* 2000; Motte *et al.* 2019). Despite this knowledge, few studies have attempted to model the trajectories of wild individuals with seasonal infection dynamics and resource availability using dynamic resource allocation models.

The overarching goal of this study is to understand how the level of pathogen infection and local seasonality interact to mediate host growth rates at early life stages (Fig. 1a). First, we

identified host strategies that maximize fitness until sexual maturity. We hypothesized that individuals at early life stages allocate energy for growth at lower infection levels but shift energy to activate and maintain immunological defenses as the pathogen-mediated damage increases. Second, we parametrized an agent-based model to follow the trajectories of individuals with seasonal infection dynamics using the energy allocation strategies that maximized fitness. We hypothesized that lower growth rates of infected individuals would result from shifts in energy allocation to immune defense (i.e., control infection), whereas higher growth rates would allow rapid reproductive maturation if the level of infection is tolerable (Fig. 1b). Third, we evaluated whether shifts in resource availability and pathogen exposure between seasons exacerbated these tradeoffs. We hypothesized that differences in growth result from the host response to severe infections, which are exacerbated during seasons characterized by decreased foraging success (Fig. 1b). Therefore, we expected increased mortality in scenarios where individuals are born during suboptimal conditions. Understanding energy allocation shifts from growth to control infection will allow us to make inferences regarding inter- and intraspecific competition, fitness effects, and survival rates. Incorporating seasonality to understand the fitness consequences of these tradeoffs is particularly important considering the global rise of emerging and re-emerging diseases due to climate change (El-Sayed & Kamel 2020). Our findings provide the modeling structure to measure mismatches in reproductive activity, food availability, and differing infection exposure within a seasonal context.

Methods

We developed two dynamic state variable models to determine the pattern of energy allocation that maximizes future fitness. Note that we used survival and body size as a proxy for future fitness under pathogen infection. We estimated the expected future fitness at the end of our time horizon: one year. The discrete state variables of interest in our models were time (t),

size (S), and level of infection (I). Given that not all individuals have the same fate within a population, we considered heterogeneity in the model by incorporating the following probabilities: obtaining different units of energy per week from foraging (E), an uninfected individual becoming infected (P_I), and the probability of dying from causes other than infection as a function of both, body size ($M_S(S)$) and the level of infection ($M_I(I)$). In the basic model, parameter values were constant across time, while in the second (hereafter, the seasonal model), the probabilities of obtaining energy (E) and of becoming infected (P_I) depended on the season (Warm/Cool). This set of generic units for variables and parameters can be applied to multiple scenarios across taxa, but their values must be relative to the specific system that is been studied (Breckling 2002; Mangel & Clark 1988).

We used available field data on the host *Eleutherodactylus coqui* and the pathogen *Batrachochytrium dendrobatidis* (*Bd*) to parameterize a two-season model (Box 1, Table 1). The host is a terrestrial species that reproduces all year around; its life history as well as the host-pathogen dynamic with *Bd* have been well characterized among seasons in nature and laboratory experiments (Box 1). We modeled frog energy allocation when faced with *Bd*-infection during development as juveniles, starting with hatching from the egg. Specifically, we identified the state-dependent allocation to growth and immune function that maximized the expected future reproductive success at the end of the time horizon. Then, with the predicted frog energy allocations that maximize future fitness, we implemented an individual-based model to simulate populations of individuals using these optimal strategies to describe the growth trajectories (Breckling 2002; Graham *et al.* 2021). We also compared between seasons by solving the model and simulating cohorts of individuals hatching at different times of the year (see below).

Building the basic model

We used life history data to establish the time horizon and the length of each time step for the model (see Box 1, Fig. 1, Table 1). We modeled the growth of individual frogs using one-week

time intervals, starting at hatching, such that the maximum time (T) was 52 weeks (Box 1). The individual frogs in this model were juveniles and early adults (young of the year). We modeled discrete size states (S) ranging from 1 to 208, corresponding to different measurable-length unit increases between juveniles and adults. Size categories were treated as fixed constants, where Unit 1 represents size upon hatching, Unit 50 represents size at reproductive maturity, and Unit 208 represents the maximum size reported for this species. At Unit 50, there is a change in growth rate for a given amount of energy to reflect that juveniles and adults grow constantly but at different rates; thus, each size state reflected an increase of 0.44 mm for juveniles and 0.22 for adults (Fig. 1a, Box 1, Guarino *et al.* 2019; Joglar 1998; Stewart & Woolbright 1996). Because we were mainly interested in juveniles' growth, we used average mean growth between sexes after maturity. The level of infection (I) was modeled logarithmically with eleven states increasing from 0 to 10, with 0 representing an uninfected individual and 1 to 10 corresponding to 10^1 to 10^{10} *Bd* zoospores. This topmost number of zoospores is greater what is previously reported for the species (Longo *et al.* 2010, 2013), but it can be used as a relative scale for tolerant species. Considering that foraging success is stochastic, we assumed frogs obtained 0, 2, or 4 generic units of useable energy (E) per week, with equal probability, after fulfilling their maintenance energy cost. Individuals must allocate these energy units to one of the three strategies: grow ($i = G$), control infection ($i = C$), or split energy between these two processes ($i = B$) (Fig. 1b). In all cases, size states (S) increased in proportion to the energy allocated to growth depending on the strategy (equation 1),

$$S_{t+1}(i) = \begin{cases} S_t + E, & \text{when } i = G \\ S_t + 0, & \text{when } i = C \\ S_t + \frac{1}{2}E, & \text{when } i = B, \end{cases} \tag{1}$$

where i represents the energy allocation strategy and E the generic energy units from foraging. Likewise, the level of infection (I) will inherently increase one unit reflecting pathogen exponential growth, which we assumed is not affected by external factors. It will only decrease

in proportion to the amount of energy allocated towards pathogen control (equation 2), and remain as 0 when the individuals do not get infected.

$$I_{t+1}(i) = \begin{cases} I_t + 1 - 0, & \text{when } i = G \\ I_t + 1 - E, & \text{when } i = C \\ I_t + 1 - \frac{1}{2}E, & \text{when } i = B. \end{cases} \quad (2)$$

In the model, we did not assume acquired immunity because the host can clear infections and be re-infected in this system. The probability of an uninfected individual becoming infected (P_I) was 0.445, which is the mean *Bd*-prevalence across the year (Box 1, Fig. S3). Although we acknowledge that growth rates are associated with temperature (Zuo *et al.* 2012; Álvarez & Nicieza 2002), we assumed constant temperature-independent growth because this relationship may obscure the effect of the food availability between seasons. An individual could clear an early infection with sustained investment in immunity but only at the expense of growth. We considered that infection levels increased the probability of host death (Longo *et al.* 2013). Thus, in addition to the probability of mortality based on size from causes independent of infection, $M_s(S)$, we also included the infection-based probability of mortality, $M_I(I)$. We modeled size-dependent mortality as a decreasing function of body size based on a log-logistic curve (equation 3, Fig. S1a),

$$M_S(S) = 1 - \left(\frac{M_H}{1 + e^{d(S - S_T)}} \right), \quad (3)$$

where M_H describes the probability of dying in the time horizon, which in our model $M_H = 0.80$ in one year. The survival probability in one year is very conservative with respect to what has been reported for adults in the species, approximately 94%, considering that juveniles' survival should be lower than adults (Stewart 1995). The probability of dying on each time step decreases as size increases at a constant rate according to equation 3 where $d = 0.05$, and where S_T is the size with the median probability of dying, in this case $S_T = 50$. An infected individual

probability of dying due to infection level ($M_I(I)$) starts at 9×10^{-5} and logarithmically increases every two levels of infection such as equation 4 (Fig. S1b),

$$M_I(I) = \begin{cases} 0, & \text{for } I = \{0\} \\ 9\times10^{-5}, & \text{for } I = \{1,2\} \\ 9\times10^{-4}, & \text{for } I = \{3,4\} \\ 9\times10^{-3}, & \text{for } I = \{5,6\} \\ 9\times10^{-2}, & \text{for } I = \{7,8\} \\ 9\times10^{-1}, & \text{for } I = \{9,10\}. \end{cases} \tag{4}$$

We assumed the expected future fitness was based on final size (*i.e.*, size at time T) and current infection such that equation 5,

$$F(S,I,T) = (1 - M_I(I))\,\frac{1}{1+e^{-0.5(S-100)}}. \tag{5}$$

The future fitness incorporates the expected benefits of being larger (S; Fig. S2) for reproduction and the probability of surviving expected due to infection ($1-M_I(I)$). The optimal state-specific strategy ($i = \{G,C,B\}$) is the one that increases expected future fitness (F), thus we calculated the fitness associated to each investment strategy (v_i) and selected the maximum value (equation 6),

$$F(S,I,t,T) = \max(v_i) \text{ where } i\{G,C,B\}. \tag{6}$$

The optimal strategy reflects how the state variables size and infection, may change from one time step to another based on the amount of energy frogs find and the energy they allocate to growth and or control the infection. Calculating v_i takes into account the probability of survival as a function of size ($1-M_S$) and infection ($1-M_I$), the probability of finding different amounts of allocatable energy units, the future fitness $F(S,I,t+1,T)$, and the probability of getting infected if uninfected (P_I). Therefore, equation 6 expanded as detailed in equations 7 and 8 for uninfected and infected individuals, respectively.

Uninfected individuals are constrained to allocate all available energy to grow, but they can become infected during that time step. Thus, $v_{i=G}$ for these uninfected individuals is as in equation 7. We solved the equation to demonstrate how size and infection change in a one-time step, as detailed below,

$$v_i(S, I=0, t, T, i=G) = 1 - M_{S(t)} \begin{cases} P_{I(t)} & \left(\begin{array}{c} p(E|E=0)\times \\ F[S_{t+1}=S_t, I_{t+1}=1, t+1] \\ +p(E|E=2)\times \\ F[S_{t+1}=S_t+2, I_{t+1}=1, t+1] \\ +p(E|E=4)\times \\ F[S_{t+1}=S_t+4, I_{t+1}=1, t+1] \end{array} \right) \text{ get infected} \\ 1-P_{I(t)} & \left(\begin{array}{c} p(E|E=0)\times \\ F[S_{t+1}=S_t, I_{t+1}=0, t+1] \\ +p(E|E=2)\times \\ F[S_{t+1}=S_t+2, I_{t+1}=0, t+1] \\ +p(E|E=4)\times \\ F[S_{t+1}=S_t+4, I_{t+1}=0, t+1] \end{array} \right) \begin{array}{c} \text{remains} \\ \text{uninfected.} \end{array} \end{cases} \tag{7}$$

The first term corresponds to the case that an individual becomes infected and refers to the individuals that survive $(1-M_S)$ and get infected during the current time step (P_I); future fitness (F) depends on the amount of allocatable energy (E). As a result, the future fitness (F[$S_{t+1,I}$, $I_{t+1,I}, t+1$]) sets the value of the state variables (S, I, t) on the next time iteration. The second term refers to those individuals that do not get infected during the current time step, indicated by the probability of not getting infected $(1-P_I)$; as a result, the level of infection remains zero.

In contrast, infected frogs will choose the strategy that maximizes the future fitness (F) among the three energy allocation strategies; thus, equation 6 expands, and changes in state variables are reflected accordingly in equation 8,

$$v_i(S, I>0, t, T, i) = (1 - M_{S(t)}) * (1 - M_{I(t)}) \begin{pmatrix} p(E|E=0)\times \\ F[S_{t+1,i}, I_{t+1,i}, t+1]+ \\ p(E|E=2)\times \\ F[S_{t+1,i}, I_{t+1,i}, t+1]+ \\ p(E|E=4)\times \\ F[S_{t+1,i}, I_{t+1,i}, t+1] \end{pmatrix} \begin{matrix} \text{for each} \\ i = \{G, C, B\}. \end{matrix} \quad (8)$$

In this equation, the probability of getting infected (P_I) is one because individuals are already infected, thus, it only has one term. However, it considers two mortality probabilities, the probability of surviving due to external causes ($1 - M_S$) and the infection ($1 - M_I$). Because infected individuals can choose among the three energy allocation strategies, the future fitness ($F[S_{t+1,I}, I_{t+1,I}, t+1]$) will depend on the energy they forage and the chosen strategy.

We solved these equations to generate a matrix of state-specific optimal decisions for all possible combinations of the three states: size, infection level, and time (Fig. 2a). Next, using state variable elements of the decision matrix, we simulated a population of 100 individuals using Monte Carlo chains to predict realized differences in growth rates, time to maturity, and survival after the growing season in populations following the optimal strategy set. We chose this population size because it is akin to the field data generated from population genomic estimates (Torres-Sánchez & Longo, 2022).

Extending the basic model to include seasonal effects

Direct-developing frogs, like many other taxa, reproduce year-round (Bignotte-Giró *et al.* 2021; Joglar 1998; Townsend & Stewart 1994), which suggests that they can experience suboptimal conditions at some point during their growing period. To examine the cost of the interaction of growing at suboptimal times and the level of infection, we generated new parameter sets for each season (Table 1), solved the models for the optimal behavior, then simulated and evaluated the effects of starting life at four points during the year. The four temporal scenarios corresponding to frogs that hatch at different times of the year differ in how the seasons occur

on the time horizon. Seasons differ in terms of the probability of becoming infected (P_I) and the probability of gaining energy (E) from foraging bouts corresponding with the seasons; two variables that are affected by the seasonality (Box 1, Table 1). We used the prevalence of infection in each season to parameterize the probability of getting infected (P_I) based on the proportion of infected individuals found each season (Box 1, Fig. S3). In addition, the number of prey and foraging success vary between seasons (Box 1). Therefore, we assigned a higher probability of acquiring more energy during the warm season, such that the probability of obtaining 0, 2, or 4 units of energy (E) per week from foraging was 0.45, 0.45, and 0.10, respectively, in the cool season and 0.10, 0.45, and 0.45, in the warm season. Changing the probability of finding none to four energy units between seasons is a simplistic way to represent the difference in the amount of energy individuals can obtain from foraging between seasons which can be scaled based on the study system without requiring more data processing capacity.

To evaluate the role of the interaction between seasonality and infections on individuals' fitness, we compared the results among four seasonal scenarios that represent frogs hatching on November–CCWW, February–CWWC, May–WWCC, and August–WCCW. Specifically, we compared among the seasonal scenarios: 1) the set of optimal strategies, 2) the relationship between growth rate (*i.e.*, differences in size states weeks 13 and one for each period divided by 13) and the mean level of infection between cool and warm seasons, and 3) three variables associated to fitness: time to maturity (S = 50), and the size and survival at the end of the simulation (t = 52). Models, simulations, and graphs were built in R (Team 2022), setting the seed number to 854354. The code is available on GitHub (https://github.com/ZuaniaColon/Modeling-costs-of-seasonal-infections.git).

Results

We found that size and level of infection influenced the selected strategy in the optimization model (Fig. 2). When infection levels were very low, the strategy that maximized fitness was to allocate all the energy to growth (Fig. 2, I = 1). When infection levels were moderate, the best strategy (except for the largest individuals) was to split energy between growing and controlling infections. In contrast, larger size classes typically defended against the pathogen (Fig. 2, I = 2:3). Finally, when levels of infections were high, most individuals, regardless of size, opted to invest exclusively in immune function (Fig. 2; I = 4:10).

Our forward simulations revealed the tolerated infection thresholds as individuals always kept levels of infection below six (Fig. 3a-e). The optimized shifts in energy allocation resulted in increased growth rates when individuals carried low infections (lighter colors) and decreased with higher ones (darker colors) (Fig. 3a). Consequently, individuals were smaller at the end of the time span of 52 weeks when their mean level of infection across time was high. In addition, we found that incorporating seasonality in our optimization model affected optimal strategies at given specific state variables (Fig. 2b-d). The best strategy to increase future fitness was to grow or grow/control infection during the warm-wet season and mainly control infection during the cool-dry season when pathogen levels were between 10^2-10^3 zoospores ($I = 2$ or 3). However, when the pathogen level reached 10^4 zoospores ($I \geq 4$), hosts allocated energy to suppress the infection, except when the frogs were near the end of their growing season (> 48 weeks) (Fig. 2). The different strategies selected in both models are also reflected in growth rates. The growth rate curve from the simulation using the optimized strategies from the basic model was linear (Fig. 3a). In contrast, the slope's steepness differed between seasons in the seasonally-explicit optimization models (Fig. 3b-e). Overall, our results showed that the seasons in which frogs hatched significantly influenced their growth trajectories.

As expected, our between-model comparisons of growth rates and mean level of infection

accurately captured the differences between models and seasons (Fig. 3f-j). In both models, the growth rate decreased with the individuals' mean level of infection. However, whereas the decrease in the basic model is constant (Fig. 3f), the slope and the intercept varied between seasons (Fig. 3g-j). For example, models showed differences in the intercept between seasons and more variation in infection intensities during the cool season (blue points on Fig. 3g-j).

Our models indicated that the best time to hatch for *E. coqui* is at the beginning of the warm season (Fig. 4; W-W-C-C). Although frogs can achieve similar sizes at the end of the growing season (Fig. 4b), they reach maturity earlier (Fig. 4a) and increase their likelihood of survival given the seasonal pattern (Fig. 4c). In contrast, the worst scenarios occurred when frogs hatched at the beginning of the cool (C-C-W-W) or at the end of the warm seasons (W-C-C-W), because fewer individuals reached maturity within one year (Fig. 4a) and the likelihood of surviving the 52 weeks was lower (Fig. 4c).

Discussion

Hosts across taxa show variation in their physiological and immunological responses to epizootics of emerging pathogens (Genersch & Aubert 2010; Huot *et al.* 2014; Kohl *et al.* 2016; Longo *et al.* 2023; Malpica *et al.* 2006; Soler *et al.* 2003; Webster *et al.* 2017; Wilder *et al.* 2011). Although mathematical models have been previously used to understand host-pathogen interactions on a population scale, our dynamic state variable approach explicitly showed what individuals must do to increase their fitness and how those decisions affect population dynamics. We demonstrated that: 1) high levels of infection trigger changes in energy allocation between growth and immunological defenses; 2) differences in energy availability between seasons exacerbate the effects of this tradeoff; and 3) this tradeoff increases time to maturity and decreased survival when individuals experienced the cool season right after hatching.

Identifying tradeoffs using dynamic optimization models

Our results suggest that individuals opted to tolerate infection as long as possible so they could invest in growth and only turned to serious defenses when infection levels were high, close to the sub-lethal threshold (Fig. 2). In nature, this pattern is expected because the cost of the immune response is higher than the cost of maintenance (Derting & Compton 2003). Individuals increased the probability of survival by allocating energy to control and/or clear the infections, but at the cost of growth, which resulted in delayed maturity (Fig. 3). Surprisingly, we did not observe a large variability in size between simulations; however, individuals with a higher mean level of infection were smaller within each simulation, suggesting that differences in growth rates can result in smaller individuals (Burrowes *et al.* 2008). These results mirror other systems where individuals exhibit elevated healing capacity at the cost of lower growth rates (Korfel *et al.* 2015). Body size and time to maturity are associated with fitness in many species, which also influences recruitment (Hilderbrand *et al.* 2019; Townsend & Stewart 1994; Wise & Jaeger 2021). Therefore, we must include future fitness when evaluating population viability after disease outbreaks.

Although our model emphasized the tradeoff between energy allocated to control the infection versus growth, we recognize that a mosaic of interacting mechanisms can result in size differences between infected and non-infected individuals. Frogs could be experiencing a downward-spiral in which infection does not allow them to acquire the appropriate energy level because their appetite or foraging success decreases with disease symptoms (Carter *et al.* 2020; Peterson *et al.* 2013; Venesky *et al.* 2009). Diversity in the immune repertoire could also increase with age, with larger individuals carrying more receptors related to acquired resistance (Savage & Zamudio 2011). We propose experiments manipulating the amount of food intake followed by pathogen exposures to confirm which mechanisms are responsible for these growth-defense tradeoffs.

Seasonality exacerbates the growth-defense tradeoffs

We expected seasonality would exacerbate differences in growth rate because host-pathogen dynamics and food availability vary by season (Longo *et al.* 2010; Stewart & Woolbright 1996). We did not find differences in frog body size at one year across models when data were analyzed at the population level; because they chose to tolerate the infection and invest in growth, which is more critical at early stages (*i.e.*, 100 individuals simulated per seasonal scenario). Because size is essential for survival and reproduction, it is common for individuals to compensate for size using two mechanisms: increasing growth rate after a period of poor nutrition and reduced growth (spline pattern driven by higher growth rates during warm seasons in Fig. 3b-e and S4b-e) or by delaying maturity (Fig. 4a) (Finkielstain *et al.* 2013; Metcalfe & Monaghan 2001). Higher temperatures during the warm season increase individual growth rate (Colón-Piñeiro 2017). Compensation for growth after a period of poor nutrition provides short-term advantages but comes at a cost, ranging from locomotion performance to reduced lifespan (reviewed in Metcalfe & Monaghan 2001). Consistent with previous studies in natural frog populations (Longo *et al.* 2010), higher levels of infections near and above $I = 4$ were only observed during the cool season when seasonality was included. Drought-related stress makes frogs more susceptible to pathogens (Longo *et al.* 2010) and *Bd* operates optimally at lower temperatures during the cool-dry season (Van Rooij *et al.* 2015). Future empirical research could help test our theoretical assumptions and predictions in these models (Grainger *et al.* 2022).

Poor parental decisions influenced future fitness traits

We demonstrated that seasonality affects frogs' time to maturity and survival (Fig. 3a-e, S2, and 4a,c), which can have carryover effects on long-term population viability (Cabrera-Guzmán *et al.* 2013). Hatching at the end of the warm season was unfavorable, probably due to synergies between the probability of dying because of the disease, size, and the high probability of getting

infected. Because parents determine the seasonal period in which eggs hatch, our models indicate that continued reproduction during the cool season results in lower fitness per offspring for the parent. We speculate that reproduction at suboptimal times can result from individuals with high fitness reproducing for a second time during the year or individuals with low fitness that could not successfully compete to mate during the warm season. Regardless of the quality of these individuals, reproduction during the warm-wet season will expose neonates to more diverse microbiomes upon hatching because adults likely host more beneficial symbionts than in the cool-dry season (Le Sage *et al.* 2021; Longo *et al.* 2015).

These interactions are particularly important for population recruitment because models predict more extreme events due to climate change (Planton *et al.* 2008; Ummenhofer & Meehl 2017). For example, prolonged droughts can severely impact animal communities, including frogs and their prey (Lister & Garcia 2018). Climate predictions anticipate dry seasons becoming longer and more irregular (Neelin *et al.* 2006; Nurse & Sem 2001; Team *et al.* 2015), and amphibians might not be able to cope with the pace of these changes. Our model approach could be a useful tool to evaluate such scenarios. These shifts can drive extinctions, especially in those species recovering from initial *Bd* outbreaks.

Potential applications of dynamic models in conservation

Our model can be extended to other endangered taxa providing key insights into conservation. Because the state variables are relative to the system, our dynamic model allows to predict interactions between different scenarios, including outbreaks and extreme droughts, by changing parameter values. Multiple agencies have been joining efforts to breed threatened species *ex-situ* for reintroduction, for example, amphibian species threatened by *Bd*; however, the success of these programs is debatable (Harding *et al.* 2016). Extensions of this model may allow researchers to predict the best time to release individuals into the wild, given a priori information about amphibian reproductive phenology, development, and infection risk.

Conclusions and future directions

Our results demonstrate that having plastic energy allocation strategies promotes survival and increases fitness under different pathogen or parasite pressures. Individuals prioritize growth over fighting infection by tolerating infection rather than sacrificing growth more than absolutely necessary. Frogs only allocated energy to control the infection at sub-lethal levels. In these cases, the latency in growth resulted in delayed maturation which can have detrimental long-term effects on fitness. Our models also demonstrated that individuals were able to slightly compensate for a "bad start" because of seasonality by growing faster during seasonal transitions or delaying maturity. Because our approach relied on mathematical models, common-garden experiments can provide additional empirical evidence for these results. For example, experiments quantifying growth while varying the amount of available food according to seasonal patterns could reveal more details on the consequences of infection across life-history stages. In addition, modeling the reproduction-defense tradeoffs in adults can be coupled with our model to increase our understanding of how pathogens drive population dynamics in different climatic scenarios across taxa. Our research demonstrates the utility of dynamic state variable models, which can be extended to multiple species and conditions (*e.g.*, extreme droughts, pathogen outbreaks, and species reintroduction for conservation) by adjusting parameter values with empirical data collected from experiments or field observations.

Acknowledgments

We thank our colleagues from the Dynamic Optimization Models course, PEERs, and the Longo Lab at UF-Biology and O. Acevedo-Charry for their input and thoughtful discussions about earlier versions of the models presented in this paper. Funding was provided by the National Science Foundation (NSF-IOS-2011281, 2011278, NSFDDIG-1310036), the Hispanic Scholarship Fund, The Society for Integrative and Comparative Biology, the Department of Biology, and the

Biodiversity Institute at the University of Florida. St. Mary's participation in this project was partially supported by the NSF IR/D program.

References

Agha, S. B., Tchouassi, D. P., Bastos, A. D. S. & Sang, R. (2017). Dengue and yellow fever virus vectors: seasonal abundance, diversity and resting preferences in three Kenyan cities. *Parasites & Vectors*, 10, 628.

Alizon, S., Hurford, A., Mideo, N. & Van Baalen, M. (2009). Virulence evolution and the trade-off hypothesis: history, current state of affairs and the future: Virulence evolution and trade-off hypothesis. *Journal of Evolutionary Biology*, 22, 245–259.

Altizer, S., Dobson, A., Hosseini, P., Hudson, P., Pascual, M. & Rohani, P. (2006). Seasonality and the dynamics of infectious diseases. *Ecology Letters*, 9, 467–484.

Alvarado-Rybak, M. & Azat, C. (2021). Chytridiomycosis outbreak in a Chilean giant frog (*Calyptocephalella gayi*) captive breeding program: Genomic characterization and pathological findings. *Frontiers in Veterinary Science*, 8, 9.

Berger, L., Speare, R. & Skerratt, L. (2005). Distribution of *Batrachochytrium dendrobatidis* and pathology in the skin of green tree frogs *Litoria caerulea* with severe chytridiomycosis. *Diseases of Aquatic Organisms*, 68, 65–70.

Bignotte-Giró, I., López-Iborra, G. M., Ramírez-Pinilla, M. P. & Fong G., A. (2021). Reproductive phenology of five species of terrestrial frogs (Genus *Eleutherodactylus*) from Cuba. *Journal of Herpetology*, 55, 127–136.

Brannelly, L. A., McCallum, H. I., Grogan, L. F., Briggs, C. J., Ribas, M. P., Hollanders, M., Sasso, T., Familiar López, M., Newell, D. A. & Kilpatrick, A. M. (2021a). Mechanisms underlying

host persistence following amphibian disease emergence determine appropriate management strategies. *Ecology Letters*, 24, 130–148.

Brannelly, L. A., Webb, R. J., Jiang, Z., Berger, L., Skerratt, L. F. & Grogan, L. F. (2021b). Declining amphibians might be evolving increased reproductive effort in the face of devastating disease. *Evolution*, 75, 2555–2567.

Breckling, B. (2002). Individual-based modelling potentials and limitations. *The Scientific World Journal*, 2, 1044–1062.

Burrowes, P. A., Longo, A. V. & Rodríguez, C. A. (2008). Potential fitness cost of *Batrachochytrium dendrobatidis* in *Eleutherodactylus coqui*, and comments on environment-related risk of infection. *Herpetotropicos*, 4, 51–57.

Cabrera-Guzmán, E., Crossland, M. R., Brown, G. P. & Shine, R. (2013). Larger body size at metamorphosis Enhances Survival, growth and Performance of young cane toads (*Rhinella marina*). *PLoS ONE*, 8, e70121.

Carter, E. D., Miller, D. L., Peterson, A. C., Sutton, W. B., Cusaac, J. P. W., Spatz, J. A., Rollins-Smith, L., Reinert, L., Bohanon, M., Williams, L. A. *et al.* (2020). Conservation risk of batrachochytrium salamandrivorans to endemic lungless salamanders. *Conservation Letters*, 13, e12675.

Colón-Piñeiro, Z. (2017). *Efecto de la temperatura sobre el desarrollo de Eleutherodactylus coqui: integración entre mecanismos que influencian el fenotipo*. Ph.D. thesis, Universidad de Puerto Rico, San Juan, Puerto Rico.

Derting, T. & Compton, S. (2003). Immune response, not immune maintenance, is energetically costly in wild white-footed mice (*Peromyscus leucopus*). *Physiological and Biochemical Zoology*, 76, 744–752.

DiRenzo, G. V., Che-Castaldo, C., Saunders, S. P., Campbell Grant, E. H. & Zipkin, E. F. (2019). Disease-structured N -mixture models: A practical guide to model disease dynamics using count data. *Ecology and Evolution*, 9, 899–909.

Drewry, G. E. (1970). The role of amphibians in the ecology of Puerto Rican rain forest. In: *The rain forest project annual report*. Puerto Rico Nuclear Center, AEC-UPR, Puerto Rico, pp. 16–63.

Dushoff, J. (1999). Host heterogeneity and disease endemicity: A moment-based approach. *Theoretical Population Biology*, 56, 325–335.

El-Sayed, A. & Kamel, M. (2020). Climatic changes and their role in emergence and re-emergence of diseases. *Environmental Science and Pollution Research*, 27, 22336–22352.

Finkielstain, G., Lui, J. & Baron, J. (2013). Catch-up growth: cellular and molecular mechanisms. *Nutrition and Growth*, 106, 100–104.

Garner, T. W. J., Walker, S., Bosch, J., Leech, S., Marcus Rowcliffe, J., Cunningham, A. A. & Fisher, M. C. (2009). Life history tradeoffs influence mortality associated with the amphibian pathogen *Batrachochytrium dendrobatidis*. *Oikos*, 118, 783–791.

Garrison, R. W. & Willig, M. R. (1996). Arboreal invertebrates. In: *The food web of a tropical rain forest*. The University of Chicago Press, Chicago and London, pp. 183–246.

Genersch, E. & Aubert, M. (2010). Emerging and re-emerging viruses of the honey bee (*Apis mellifera* L.). *Veterinary Research*, 41, 54.

Graham, M., Ayabina, D., Lucas, T. C., Collyer, B. S., Medley, G. F., Hollingsworth, T. D. & Toor, J. (2021). SCHISTOX: An individual based model for the epidemiology and control of schistosomiasis. *Infectious Disease Modelling*, 6, 438–447.

Grainger, T. N., Senthilnathan, A., Ke, P.-J., Barbour, M. A., Jones, N. T., DeLong, J. P., Otto, S. P., O'Connor, M. I., Coblentz, K. E., Goel, N., Sakarchi, J., Szojka, M. C., Levine, J. M. & Germain, R. M. (2022). An empiricist's guide to using ecological theory. *The American Naturalist*, 199, 1–20.

Grogan, L. F., Humphries, J. E., Robert, J., Lanctôt, C. M., Nock, C. J., Newell, D. A. & McCallum, H. I. (2020). Immunological aspects of chytridiomycosis. *Journal of Fungi*, 6, 234.

Guarino, F. M., Crottini, A., Mezzasalma, M., Randrianirina, J. E. & Andreone, F. (2019). A skeletochronological estimate of age and growth in a large riparian frog from Madagascar (Anura, Mantellidae, *Mantidactylus*). *Herpetozoa*, 32, 39–44.

Guyer, C. (1988). Food supplementation in a tropical mainland anole, *Norops humilis*: effects on individuals. *Ecology*, 69, 362–369.

Harding, G., Griffiths, R. A. & Pavajeau, L. (2016). Developments in amphibian captive breeding and reintroduction programs. *Conservation Biology*, 30, 340–349.

Hilderbrand, G. V., Gustine, D. D., Joly, K., Mangipane, B., Leacock, W., Cameron, M. D., Sorum, M. S., Mangipane, L. S. & Erlenbach, J. A. (2019). Influence of maternal body size, condition, and age on recruitment of four brown bear populations. *Ursus*, 29, 111.

Huang, Q.-C., Zhang, S., Du, T., Yang, Q., Chi, S., Liu, H., Yang, Y., Dong, X. & Tan, B. (2020). Modulation of growth, immunity and antioxidant-related gene expressions in the liver and intestine of juvenile *Sillago sihama* by dietary vitamin C. *Aquaculture Nutrition*, 26, 338–350.

Huot, B., Yeo, J., Montgomery, B. L. & He, S. Y. (2014). Growth–defense tradeoffs in plants: A balancing act to optimize fitness. *Molecular Plant*, 7, 1267–1287.

Joglar, R. J. (1998). *Los coquies de Puerto Rico: su historia natural y conservación*. 1st edn. Editorial de la Universidad de Puerto Rico, San Juan.

Keehnen, N. L. P., Kučerová, L., Nylin, S., Theopold, U. & Wheat, C. W. (2021). Physiological tradeoffs of immune response differs by infection type in *Pieris napi*. *Frontiers in Physiology*, 11, Article 576797.

Kohl, W. T., McClure, T. I. & Miner, B. G. (2016). Decreased temperature facilitates short-term sea star wasting disease survival in the keystone intertidal sea star *Pisaster ochraceus*. *PLOS ONE*, 11, e0153670.

Korfel, C. A., Chamberlain, J. D. & Gifford, M. E. (2015). A test of energetic trade-offs between growth and immune function in watersnakes. *Oecologia*, 179, 343–351.

Langhammer, P. F., Burrowes, P. A., Lips, K. R., Bryant, A. B. & Collins, J. P. (2014). Susceptibility to the amphibian chytrid fungus varies with ontogeny in the direct-developing frog, *Eleutherodactylus coqui*. *Journal of Wildlife Diseases*, 50, 438–446.

Le Sage, E. H., LaBumbard, B. C., Reinert, L. K., Miller, B. T., Richards-Zawacki, C. L., Woodhams, D. C. & Rollins-Smith, L. A. (2021). Preparatory immunity: Seasonality of mucosal skin defences and *Batrachochytrium* infections in southern leopard frogs. *Journal of Animal Ecology*, 90, 542–554.

Lister, B. C. & Garcia, A. (2018). Climate-driven declines in arthropod abundance restructure a rainforest food web. *PNAS*, 115, E10397–E10406.

Longo, A. V., Burrowes, P. & Joglar, R. (2010). Seasonality of *Batrachochytrium dendrobatidis* infection in direct-developing frogs suggests a mechanism for persistence. *Diseases of Aquatic Organisms*, 92, 253–260.

Longo, A. V. & Burrowes, P. A. (2010). Persistence with chytridiomycosis does not assure survival of direct-developing frogs. *EcoHealth*, 7, 185–195.

Longo, A. V., Lips, K. R. & Zamudio, K. R. (2023). Evolutionary ecology of host competence after a chytrid outbreak in a naive amphibian community. *Philosophical Transactions of the Royal Society B*, 378, 20220130.

Longo, A. V., Ossiboff, R. J., Zamudio, K. R. & Burrowes, P. A. (2013). Lability in host defenses: terrestrial frogs die from chytridiomycosis under enzootic conditions. *Journal of Wildlife Diseases*, 49, 197–199.

Longo, A. V., Savage, A. E., Hewson, I. & Zamudio, K. R. (2015). Seasonal and ontogenetic variation of skin microbial communities and relationships to natural disease dynamics in declining amphibians. *Royal Society Open Science*, 2, 140377.

Malpica, J. M., Sacristán, S., Fraile, A. & García-Arenal, F. (2006). Association and host selectivity in multi-host pathogens. *PLoS ONE*, 1, e41.

Mangel, M. & Clark, C. W. (1988). *Dynamic modeling in behavioral ecology*. Princeton University Press, New Jersey, USA.

McCauley, S. J., Bouchard, S. S., Farina, B. J., Isvaran, K., Quader, S., Wood, D. W. & St. Mary, C. M. (2000). Energetic dynamics and anuran breeding phenology: insights from a dynamic game. *Behavioral Ecology*, 11, 429–436.

McNamara, J. M. & Houston, A. I. (1986). The common currency for behavioral decisions. *The American Naturalist*, 127, 358–378.

Merino, S., Møller, A. P. & De Lope, F. (2000). Seasonal changes in cell-mediated immunocompetence and mass gain in nestling barn swallows: a parasite-mediated effect? *Oikos*, 90, 327–332.

Metcalfe, N. B. & Monaghan, P. (2001). Compensation for a bad start: grow now, pay later? *Trends in Ecology & Evolution*, 16, 254–260.

Miller, M., White, A. & Boots, M. (2005). The evolution of host resistance: Tolerance and control as distinct strategies. *Journal of Theoretical Biology*, 236, 198–207.

Motte, C., Rios, A., Lefebvre, T., Do, H., Henry, M. & Jintasataporn, O. (2019). Replacing Fish Meal with Defatted Insect Meal (Yellow Mealworm Tenebrio molitor) Improves the Growth and Immunity of Pacific White Shrimp (*Litopenaeus vannamei*). *Animal*, 9, 258.

Neelin, J. D., Münnich, M., Su, H., Meyerson, J. E. & Holloway, C. E. (2006). Tropical drying trends in global warming models and observations. *Proceedings of the National Academy of Sciences*, 103, 6110–6115.

Nelson, R. J. (2004). Seasonal immune function and sickness responses. *Trends in Immunology*, 25, 187–192.

Nguyen, A., Mahaffy, J. & Vaidya, N. K. (2019). Modeling transmission dynamics of lyme disease: Multiple vectors, seasonality, and vector mobility. *Infectious Disease Modelling*, 4, 28–43.

Nurse, L. & Sem (2001). Small islands states. In: *Climate Change 2001: Impacts, Adaptation & Vulnerability* (eds. McCarthy, J., Canziani, O., Leary, N., Dokken, D. & White, K.). Cambridge University Press, pp. 842–875.

Peterson, J. D., Steffen, J. E., Reinert, L. K., Cobine, P. A., Appel, A., Rollins-Smith, L. & Mendonça, M. T. (2013). Host stress response is important for the pathogenesis of the deadly amphibian disease, chytridiomycosis, in *Litoria caerulea*. *PLoS ONE*, 8, e62146.

Planton, S., Déqué, M., Chauvin, F. & Terray, L. (2008). Expected impacts of climate change on extreme climate events. *Philosophical Transactions of the Royal Society B: Biological Sciences*, 340, 564–574.

Pough, F. H., Taigen, T. L., Stewart, M. M. & Brussard, P. F. (1983). Behavioral modification of evaporative water loss by a Puerto Rican frog. *Ecology*, 64, 244–252.

Rumschlag, S. L. & Boone, M. D. (2020). Lethal and sublethal amphibian host responses to *Batrachochytrium dendrobatidis* exposure are determined by the additive influence of host resource availability. *Journal of Wildlife Diseases*, 56, 338–349.

Savage, A. E. & Zamudio, K. R. (2011). MHC genotypes associate with resistance to a frog-killing fungus. *Proceedings of the National Academy of Sciences*, 108, 16705–16710.

Schiesari, L., Peacor, S. D. & Werner, E. E. (2006). The growth–mortality tradeoff: evidence from anuran larvae and consequences for species distributions. *Oecologia*, 149, 194–202.

Shudo, E. & Iwasa, Y. (2004). Dynamic optimization of host defense, immune memory, and post-infection pathogen levels in mammals. *Journal of Theoretical Biology*, 228, 17–29.

Simon, M. W., Barfield, M. & Holt, R. D. (2022). When growing pains and sick days collide: infectious disease can stabilize host population oscillations caused by stage structure. *Theoretical Ecology*, 15, 285–309.

Soler, J. J., Neve, L. d., Pérez–Contreras, T., Soler, M. & Sorci, G. (2003). Trade-off between immunocompetence and growth in magpies: an experimental study. *Proceedings of the Royal Society of London. Series B: Biological Sciences*, 270, 241–248.

Stearns, S. C. (2000). Life history evolution: successes, limitations, and prospects. *Naturwissenschaften*, 87, 476–486.

Stephenson, J. F., Young, K. A., Fox, J., Jokela, J., Cable, J. & Perkins, S. E. (2017). Host heterogeneity affects both parasite transmission to and fitness on subsequent hosts. *Philosophical Transactions of the Royal Society B: Biological Sciences*, 372, 20160093.

Stewart, M. M. (1995). Climate driven population fluctuations in rain forest frogs. *Journal of Herpetology*, 29, 437–446.

Stewart, M. M. & Woolbright, L. L. (1996). Amphibians. In: *The food web of a tropical rain forest*, 1st edn. The University of Chicago Press, Chicago. ISBN 0-226-70600-1, pp. 273–320.

Team, C. W., Pachauri, R. K. & Mayer, L., eds. (2015). *Climate change 2014: synthesis report*. Intergovernmental Panel on Climate Change, Geneva, Switzerland. ISBN 978-92-9169-143-2.

Team, R. C. (2022). R: A language and environment for statistical computing. URL `http://www.R-project.org/`.

Torres-Sánchez, M. & Longo, A. V. (2022). Linking pathogen–microbiome–host interactions to explain amphibian population dynamics. *Molecular Ecology*, 31, 5784–5794.

Townsend, D. S. & Stewart, M. M. (1994). Reproductive ecology of the Puerto Rican frog *Eleutherodactylus coqui*. *Journal of Herpetology*, 28, 34.

Townsend, D. S., Stewart, M. M. & Pough, F. H. (1984). Male parental care and its adaptive significance in a neotropical frog. *Animal Behaviour*, 32, 421–431.

Townsend, D. S., Stewart, M. M., Pough, F. H. & Brussard, P. F. (1981). Internal fertilization in an oviparous frog. *Science*, 212, 469–471.

Ummenhofer, C. C. & Meehl, G. A. (2017). Extreme weather and climate events with ecological relevance: a review. *Philosophical Transactions of the Royal Society B: Biological Sciences*, 372, 1–13.

Van Rooij, P., Martel, A., Haesebrouck, F. & Pasmans, F. (2015). Amphibian chytridiomycosis: a review with focus on fungus-host interactions. *Veterinary Research*, 46, 137.

Venesky, M. D., Parris, M. J. & Storfer, A. (2009). Impacts of *Batrachochytrium dendrobatidis* infection on tadpole foraging performance. *EcoHealth*, 6, 565–575.

576 Webster, J. P., Borlase, A. & Rudge, J. W. (2017). Who acquires infection from whom and how?
577 Disentangling multi-host and multi-mode transmission dynamics in the 'elimination' era.
578 *Philosophical Transactions of the Royal Society B: Biological Sciences*, 372, 20160091.

579 Wilder, A. P., Frick, W. F., Langwig, K. E. & Kunz, T. H. (2011). Risk factors associated with mortal-
580 ity from white-nose syndrome among hibernating bat colonies. *Biology Letters*, 7, 950–953.

581 Wise, S. E. & Jaeger, R. G. (2021). Maternal body size and condition predict measures of repro-
582 ductive success and future reproductive allocation in territorial eastern red-backed salaman-
583 ders. *Ichthyology & Herpetology*, 109.

584 Woolbright, L. L. (1983). Sexual selection and size dimorphism in anuran Amphibia. *The Amer-*
585 *ican Naturalist*, 121, 110–119.

586 Woolbright, L. L. & Stewart, M. M. (1987). Foraging success of the tropical frog, *Eleutherodacty-*
587 *lus coqui*: The cost of calling. *Copeia*, 1987, 69–75.

588 Zuo, W., Moses, M. E., West, G. B., Hou, C. & Brown, J. H. (2012). A general model for effects
589 of temperature on ectotherm ontogenetic growth and development. *Proceedings of the Royal*
590 *Society B: Biological Sciences*, 279, 1840–1846.

591 Álvarez, D. & Nicieza, A. G. (2002). Effects of induced variation in anuran larval development on
592 postmetamorphic energy reserves and locomotion. *Oecologia*, 131, 186–195.

Box 1

Natural history: *Eleutherodactylus coqui*, the coqui, is a tropical direct-developing frog endemic to Puerto Rico. Direct-developing frogs evolved to bypass the tadpole stage and emerge from the egg as miniature adults in terrestrial environments. Reproduction occurs throughout the entire year (Bignotte-Giró *et al.* 2021; Joglar 1998; Townsend & Stewart 1994), fertilization is internal (Townsend *et al.* 1981), and male parents take care of the clutch during the entire pre-hatching developmental period and even a few days after hatching (Joglar 1998; Townsend *et al.* 1984). Thus, we expect fitness costs to have their greatest effects during early life-history stages, particularly when newborn frogs hatch at suboptimal times. The likelihood of survival in juveniles is further diminished by environmental stress because individual mortality is expected after prolonged dry periods of five days (Stewart 1995). Coqui frogs hatch at a snout-to-vent length (SVL) of 6 mm on average and take approximately nine months to one year to reach maturity (Joglar 1998; Woolbright 1983) at ≈ 28 mm, independent of sex (Colón-Piñeiro 2017; Stewart & Woolbright 1996; Townsend & Stewart 1994). Like many amphibians, coquis constantly grow until reaching sexual maturity, when growth rates decrease and vary between sexes (Guarino *et al.* 2019; Stewart & Woolbright 1996); the maximum size reported for an adult female is 63 mm (Joglar 1998J). In addition, parental care can increase infection risk of the offspring due to close contact of newborns with sloughing skin from the male.

Despite less drastic temperature changes in the tropics than in temperate zones, the diversity and abundance of amphibians' prey change over time (Garrison & Willig 1996). Likewise, field studies have demonstrated reduced stomach content of tropical frogs during the dry season (Pough *et al.* 1983; Stewart & Woolbright 1996; Woolbright & Stewart 1987). Collectively, these findings suggest seasonal differences in resource availability for coqui frogs.

Host-pathogen dynamics: In our previous studies, we have primarily shown pathogen infection affecting adult mortality, but identified infected juveniles as a vulnerable life-history stage

(Langhammer *et al.* 2014; Longo & Burrowes 2010; Longo *et al.* 2015). Coqui frogs can become reinfected after clearing the pathogen, suggesting no acquired immunity (unpublished data, Longo & Burrowes). The coqui-*Bd* interactions vary between seasons, where the prevalence of infection is higher during the warm periods (unpublished data, Longo & Burrowes). *Bd*-infected frogs are expected to be more prevalent when water is available because the fungus has an aquatic zoospore that takes around five days to complete its life cycle (Berger *et al.* 2005; Van Rooij *et al.* 2015). However, identifying the mortality threshold and associated level of infection is difficult in the field. We have quantified 10^{10} *Bd* ITS copies from individuals in natural populations (unpublished data, Longo & Burrowes), and moribund individuals have been reported with a level of infection as low as 10^4 and 10^5 zoospores (Longo *et al.* 2013). Finally, infection with *Bd* is more common in smaller-sized adults in nature (Burrowes *et al.* 2008), suggesting infected direct-developing frogs incur a tradeoff between growth and immune response.

Table 1: Description of parameters used in the models and associated values.

Parameter	Description	Values
t	Time steps reflecting an increase of one week each for one year. It also indicates the current time step.	{1:52} for 1:52 weeks
$t+1$	Indicates the next time step.	{2:52} for weeks 2:52
S	Size states, each reflecting an increase of 0.44 mm in juveniles and 0.22 mm in adults SVL (snout-to-vent length).	juveniles {1:50} for 6:28mm adults {51:208} for 28:63mm
I	Level of infection reflecting a tenfold increase in the number of *Bd*-zoospores as a measure of the pathogen burden.	{0:10} where 0 = non-infected {1:10} = $(10^1 : 10^{10})$ zoospores
i	Strategies to allocate their available energy each week.	$\{G, C, B\}$, where G = Grow C = Control infection B = Grow / control infection
E	Weekly energy units obtained from foraging based on probability as a function of the model and season.	{0, 2, 4} energy generic units No season = {0.33, 0.33, 033} Cool season = {0.45, 0.45, 0.1} Warm season = {0.1, 0.45, 0.45}
P_I	Probability of an uninfected individual becoming infected.	No season = 0.45 Cool season = 51 Warm season = 39
$M_S(S)$	Probability of dying due to causes other than the infection estimated as a function of size.	Defined in equation 3
d	Decreasing constant rate of the probability of dying as a function of size.	0.05
S_T	Constant indicating the size at the mid probability of dying.	50
M_I	Probability of dying due to the level of infection, the value increases onefold every two levels of infection.	{0:10^{-1}} where $MI_0 = 0$, $MI_{1:2} = 9 * 10^{-5}$, $MI_{3:4} = 9 * 10^{-4}$, $MI_{5:6} = 9 * 10^{-3}$, $MI_{7:8} = 9 * 10^{-2}$, $MI_{9:10} = 9 * 10^{-1}$

Figure legends

Figure 1. Diagram illustrating: (**a**) expected growth rates at different life stages and (**b**) the grow-defense tradeoff hypotheses during the time horizon examined using dynamic optimization models. In **a**, juveniles grow at a constant rate independently of sex, growth rate decreases after maturity, and it can vary between sexes. Because we focused on the development of juveniles, we used the mean growth rate (dashed line). The growth rate graph was adapted for *E. coqui* from Joglar (1998). In **b**, differences in prey diversity and abundance between seasons determine energy intake, and the difference in pathogen spreading capacity influences the probability of an uninfected individual to become infected. Whereas, the infection status affects energy allocation towards growth or pathogen defense. As a result, growth rate will be higher when individuals allocate all their energy to grow, thus reaching maturity earlier. The arrows' width is proportional to the amount of energy intake allocated to each process. Words in grey indicate no energy allocated to the process, and the relative size of the frogs illustrates growth rates.

Figure 2. Decision matrices for different infection levels and seasonal scenarios. Our models include the basic model (**a**) and different seasonal scenarios (**b-d**) in which the cool (C) and warm (W) periods are alternated. Colors indicate the best strategies to increase future fitness generated by the model. Each graph's size states increase from the bottom to the top (0-208) and time from left to right (1-52 wks). For the level of infection, 0 indicates uninfected, and 1 to 10 corresponds to 10^1 to 10^{10} *Bd* zoospores. Each panel corresponds to a specific level of infection for each model-scenario combination.

Figure 3. Forward simulations (**a-e**) and the relationship between growth rate and mean level of infection (**f-j**) based on optimized strategies for 100 individuals inferred by the basic (**a** and **f**) and seasonal (**b-e** and **g-j**) models. Parameter values change based on the model and seasonal scenarios in which the cool (C) and warm (W) seasons are alternated. Each line in (**a-e**)

represents one single frog, the colors indicate the level of infection at each time step, and the (x) shows when the individual died. Vertical grey lines separate the year into four periods of 13 weeks, which in the seasonal model correspond to a specific season; dashed-horizontal lines indicate the size state at which individuals reach maturity (S=50). Solid black lines track the mean growth rate trend for each simulation. Each point in **f-j** represents a period of 13 weeks for each individual.

Figure 4. Fitness-related values for the *basic* (No seasons) and the *seasonality* models including: (**a**) time to maturity, (**b**) size at week 52, and (**c**) percentage of individuals surviving in week 52. Data correspond to the forward simulations of the dynamic optimization models with 100 individuals per simulation for the base and seasonality models, including seasonal alternations between cool (C) and warm (W) periods. Larger black points in (**a**) and (**b**) indicate the mean values, and the *n* values in (**a**) are the number of individuals that reached maturity.

Figure S1. Probability of dying as a function of discrete (**a**) size–S and (**b**) infection–I states based on equations 3 and 4, respectively. The probability of dying as a function of size is due to natural causes and not based on the level of infection. Note they are in a $\log_{10}$ scale.

Figure S2. Forward simulations (**a-e**) based on optimized strategies for 100 individuals inferred by the *basic* (No seasons) (**a**) and *seasonal* (**b-e**) models using the size of the individuals (snout-to-vent length – SVL) instead of the size states of the model. We calculated size based on the following formulas: for size states $\geq 50[(S-1)*0.44+6]$ and for size states $>50[6+(49*0.44)+(S-50)*0.22)]$. Parameter values change based on the model and seasonal scenarios in which the cool (C) and warm (W) seasons are alternated. Each line represents one single frog, the colors indicate the level of infection at each time step, and the (x) shows when the individual died. Vertical grey lines separate the year into four periods of 13 weeks, which in the seasonal model correspond to a specific season; dashed-horizontal lines indicate the size state at which individuals reach maturity (SVL=28).

Figure S3. Prevalence of *Bd*-infected individuals at Palo Colorado Forest in El Yunque, Puerto

Rico. Prevalence was calculated by monthly sampling for over a year (unpublished data, Longo & Burrowes).

Figure S4. Forward simulations based on optimized strategies for 100 individuals inferred by the *basic* (No seasons) (**a**) and *seasonal* (**b-e**) models. Parameter values change based on the model and seasonal scenarios in which the cool (C) and warm (W) seasons are alternated. Each line represents one single frog, the colors indicate the level of infection at each time step, and the (x) shows when the individual died. Vertical grey lines separate the year into four periods of 13 weeks, which in the seasonal model correspond to a specific season; dashed-horizontal lines indicate the size state at which individuals reach maturity (S=50).

Figure 1:

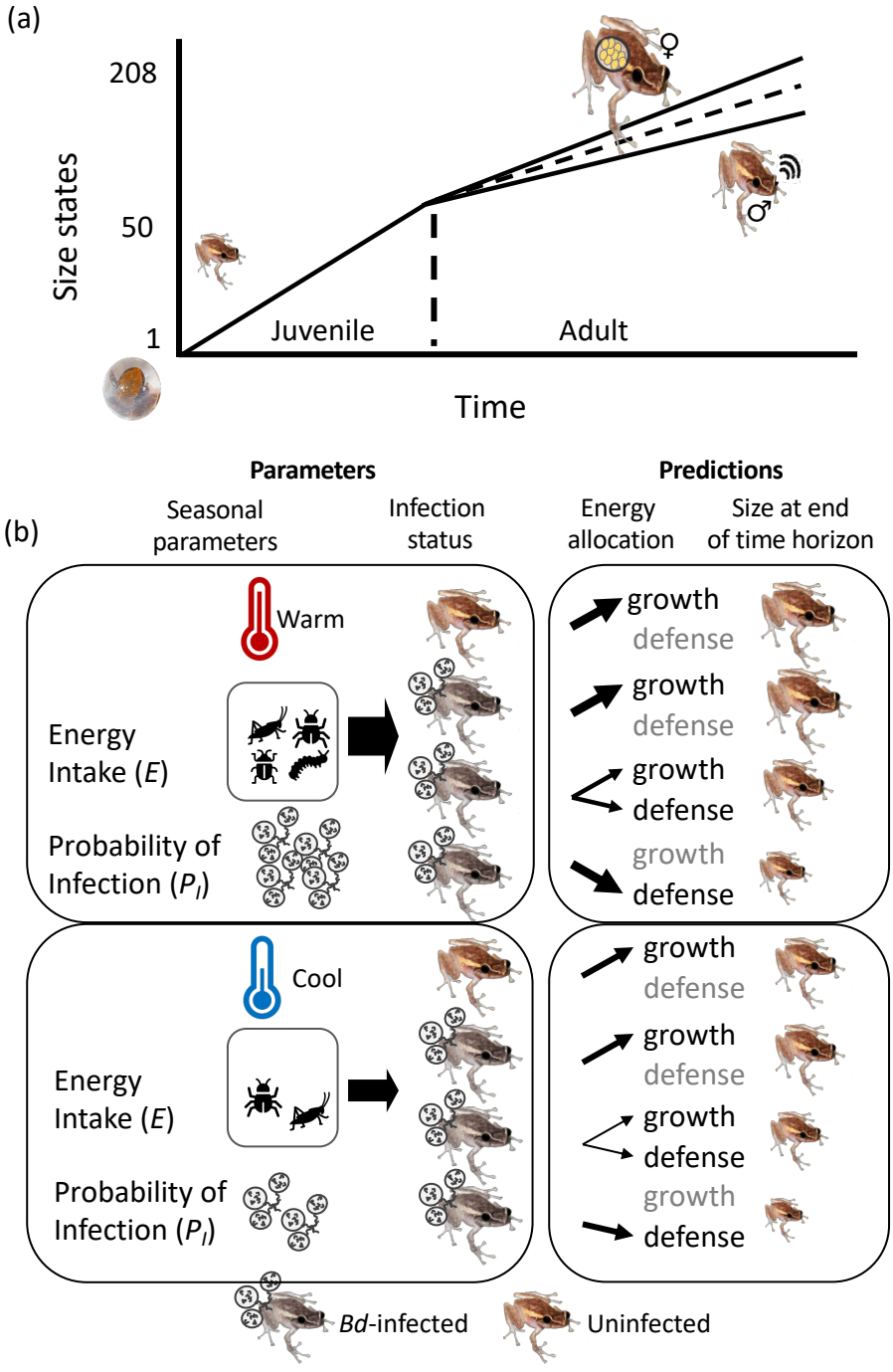
(a)
208
50
1
Size states
Juvenile
Adult
Time
♀
♂
(b)
Parameters
Predictions
Seasonal parameters
Infection status
Energy allocation
Size at end of time horizon
Warm
Energy Intake (E)
Probability of Infection (P_I)
growth
defense
Cool
Bd-infected
Uninfected

Figure 2:

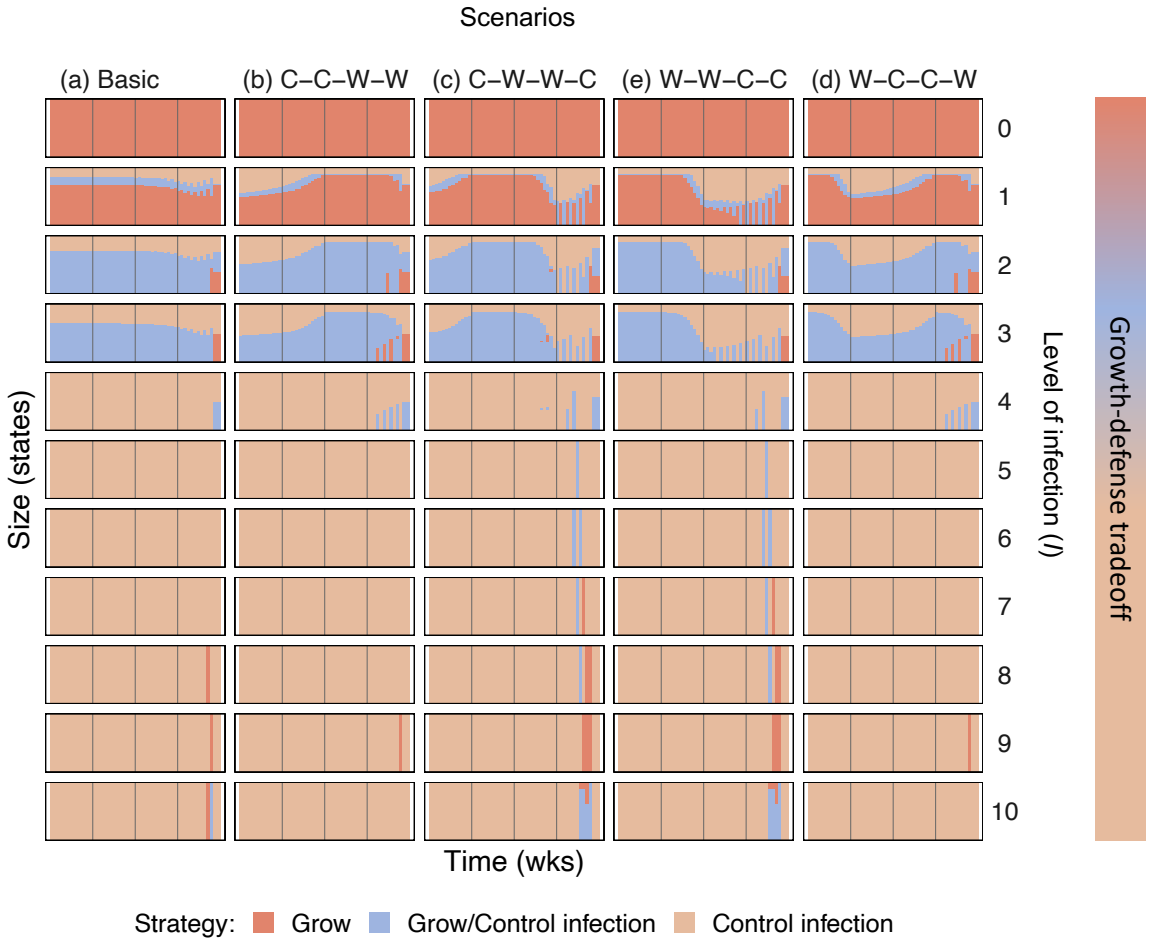
Scenarios
(a) Basic
(b) C–C–W–W
(c) C–W–W–C
(e) W–W–C–C
(d) W–C–C–W
Size (states)
Time (wks)
Level of infection (l)
0
1
2
3
4
5
6
7
8
9
10
Growth-defense tradeoff
Strategy:
Grow
Grow/Control infection
Control infection

Figure 3:

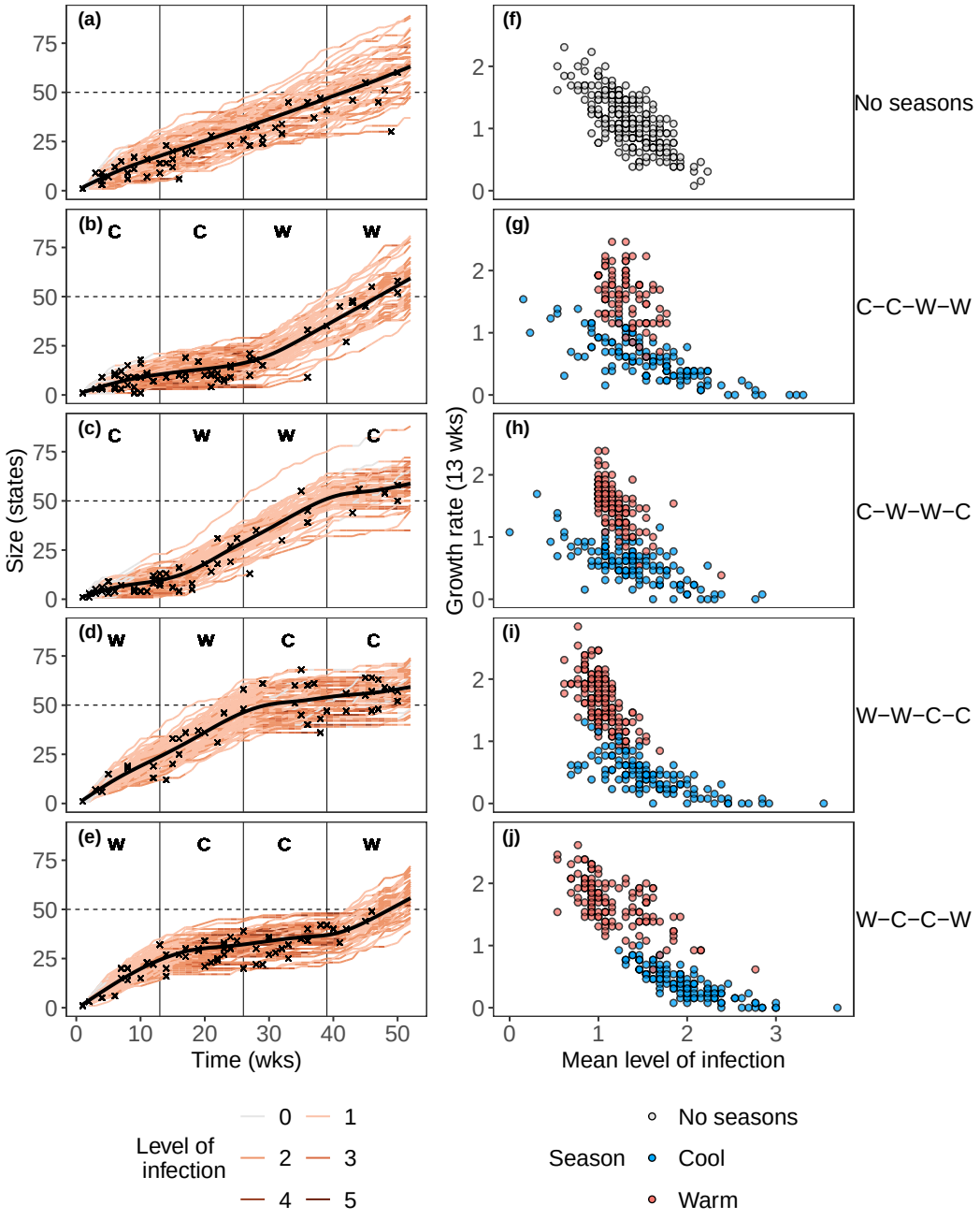
(a)
(b)
(c)
(d)
(e)
(f)
(g)
(h)
(i)
(j)
C
W
Size (states)
Time (wks)
Growth rate (13 wks)
Mean level of infection
No seasons
C−C−W−W
C−W−W−C
W−W−C−C
W−C−C−W
Level of infection
0
1
2
3
4
5
Season
No seasons
Cool
Warm

Figure 4:

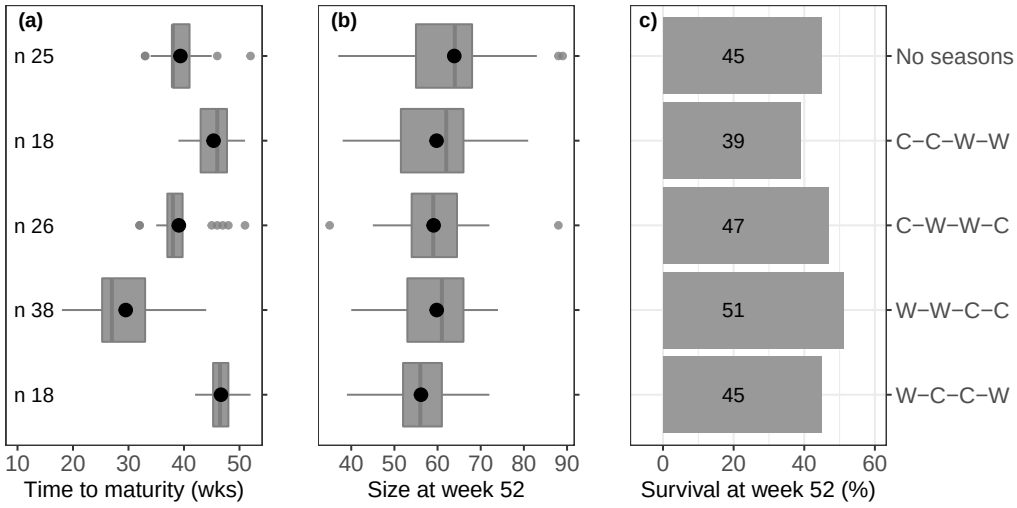
(a)
n 25
n 18
n 26
n 38
n 18
10 20 30 40 50
Time to maturity (wks)
(b)
40 50 60 70 80 90
Size at week 52
c)
45
39
47
51
45
No seasons
C−C−W−W
C−W−W−C
W−W−C−C
W−C−C−W
0 20 40 60
Survival at week 52 (%)

Figure S1:

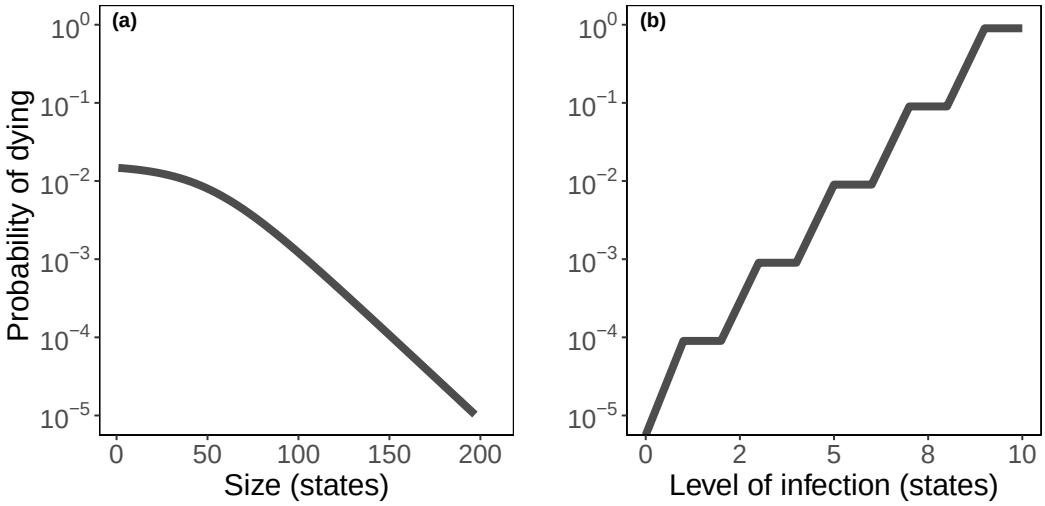
(a)
(b)
Probability of dying
10^{0}
10^{-1}
10^{-2}
10^{-3}
10^{-4}
10^{-5}
0
50
100
150
200
Size (states)
0
2
5
8
10
Level of infection (states)

Figure S2:

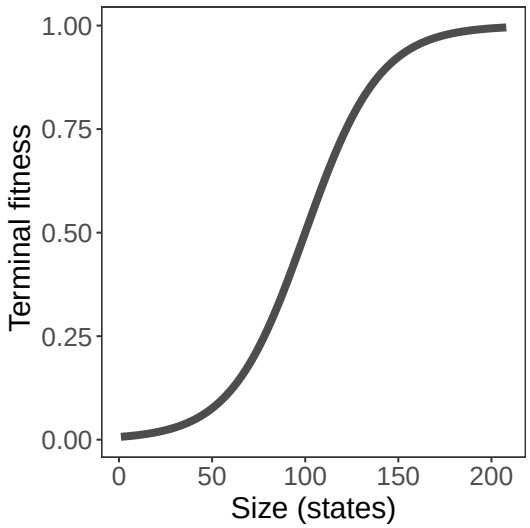
1.00
0.75
0.50
0.25
0.00
Terminal fitness
0
50
100
150
200
Size (states)

Figure S3:

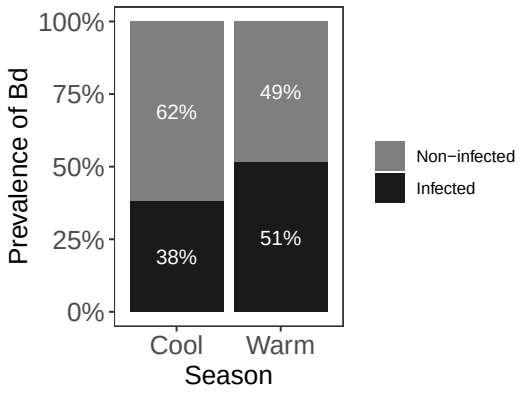
100%
75%
50%
25%
0%
Prevalence of Bd
62%
38%
49%
51%
Cool
Warm
Season
Non−infected
Infected

Figure S4:

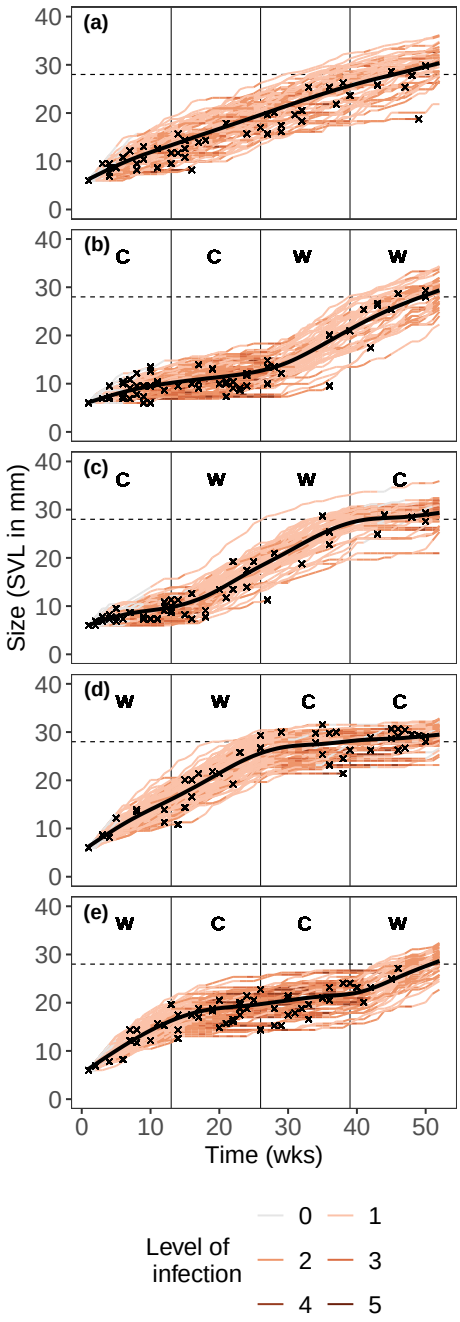
(a)
(b) C C W W
(c) C W W C
(d) W W C C
(e) W C C W
Size (SVL in mm)
Time (wks)
Level of infection
0
1
2
3
4
5